Wake-sleep transition as a noisy bifurcation

Dong-Ping Yang,[1,2,*] Lauren McKenzie-Sell,[1] Angela Karanjai,[1] and P. A. Robinson[1,2]
[1]*School of Physics, University of Sydney, New South Wales 2006, Australia*
[2]*Center for Integrative Brain Function, University of Sydney, New South Wales 2006, Australia*
(Received 1 February 2016; published 15 August 2016)

A recent physiologically based model of the ascending arousal system is used to analyze the dynamics near the transition from wake to sleep, which corresponds to a saddle-node bifurcation at a critical point. A normal form is derived by approximating the dynamics by those of a particle in a parabolic potential well with dissipation. This mechanical analog is used to calculate the power spectrum of fluctuations in response to a white noise drive, and the scalings of fluctuation variance and spectral width are derived versus distance from the critical point. The predicted scalings are quantitatively confirmed by numerical simulations, which show that the variance increases and the spectrum undergoes critical slowing, both in accord with theory. These signals can thus serve as potential precursors to indicate imminent wake-sleep transition, with potential application to safety-critical occupations in transport, air-traffic control, medicine, and heavy industry.

DOI: 10.1103/PhysRevE.94.022412

I. INTRODUCTION

The arousal state of the mammalian brain is governed by the ascending arousal system (AAS), which projects from the brainstem and hypothalamus to determine the overall arousal state of the brain [1,2]. The AAS is driven by homeostatic and circadian inputs, which are ultimately determined by influences such as light exposure and the dynamics of metabolic byproducts that favor sleep [1,3,4].

The AAS normally has two stable states, one corresponding to sleep and one to wake. The slow dynamics of circadian and homeostatic drives combine to move the system around a hysteresis loop that links these two states, with rapid transitions between them. Physiologically based modeling implies that these transitions correspond to saddle-node bifurcations [5,6].

It is of great importance to have warning of imminent transitions, particularly from wake to sleep, because of their critical safety implications for workers in the transport industry, air traffic control, and other safety-sensitive occupations. Although some vigilance classifications for alertness in the approach to wake-sleep transitions exist based on electrooculography [7] or self-assessment on scales like the Karolinska Sleepiness Scale (KSS) [8], these are subjective, not physiologically based, and/or are artificially discretized. Better quantitative understanding of precursors to this transition would be highly valuable, and critical fluctuations as it is approached may correspond to such phenomena as microsleeps, in which drivers and other workers momentarily doze off for a few seconds at a time [9–11]. Indeed, fatigue and sleep-related attentional and performance lapses are believed to account for up to 50% of traffic accidents, for example [9,12].

Recent advances in understanding the AAS have allowed a number of mathematical models of arousal dynamics to be developed [1,5,13–26]. In particular, the physiologically based model of Phillips and Robinson [5] has had its parameters rigorously constrained and has been successfully applied to a wide variety of phenomena, including normal sleep-wake cycles [5,27], sleep deprivation and recovery [28,29], circadian entrainment and jetlag [4], the effects of caffeine [30], and varieties of mammalian sleep patterns [31], as summarized in a recent review [6].

Phenomena in which slow dynamics are followed by a sudden transition from one stable state (e.g., wake) to another (e.g., sleep) are examples of critical transitions that occur in a wide range of complex systems [32], including earthquakes [33,34], climate tipping [35–39], and wire creep under stress [40]. The changes at such transitions are drastic, and of great practical importance, so early-warning signals have been sought across all these fields. Table 1 in Ref. [41] illustrates the range of fields in which these catastrophic bifurcations occur, including early-warning indicators investigated to date, which include such measures as variance, autocorrelation, skewness, and others. This table includes one other neurological application (to epilepsy [42]), but these methods have not yet been rigorously applied to the wake-sleep transition.

At a critical transition via a saddle-node bifurcation, a fixed point of the system ceases to exist, which corresponds to the disappearance of a minimum in a potential energy function [43,44], which is often expressed in a standardized normal form in dimensionless variables. As this point is approached in the presence of noise in the system, the variance of fluctuations around the fixed point increases, while their spectral width decreases due to critical slowing [40,41,45]. The scaling of the variance with the distance from the critical point has been predicted, but not yet fully tested, whereas the scaling of the spectral width has not yet been analyzed [40].

Existing physiologically based models of arousal dynamics typically contain many biophysical parameters and must be simplified in order to make tractable contact with the more abstract normal-form analyses typically used to explore critical transitions in the literature. However, it is essential to retain the ability to relate the results back to the actual brain and its dynamics, so any nondimensionalization or rescaling of variables needs to be explicit and invertible.

In this paper, we employ the Phillips-Robinson model [5] to investigate the early-warning signals of the wake-sleep transition, where the disappearance of the stable wake state pushes the system towards sleep. In Ref. [44] this model was written in terms of an approximate potential function, which

*dp.yang@sydney.edu.au

is adapted in the present work. In this approximation, the normal form of dynamics is written in terms of the motion of a particle in a potential well with friction. In Sec. II we briefly describe the Phillips-Robinson model and its relation to the underlying physiology. Then we present the theoretical analysis in Sec. III, including simplification of the model to dimensionless form, derivation of the normal form near the critical point, calculation of the underlying potential function for the saddle-node bifurcation, determination of the power spectrum, and prediction of scalings. In Sec. IV the theoretical predictions of the power spectrum and scalings are compared with the numerical simulation results with white noise drives. Finally, the results and future avenues for application of this work are discussed in Sec. V.

II. PHYSIOLOGICAL MODEL OF THE AAS

The main components of AAS and their interactions are shown in Fig. 1. The core of the wake-sleep switch consists of the monoaminergic brainstem nuclei (MA) and the ventrolateral preoptic nucleus (VLPO), which inhibit each other so that the MA is active and the VLPO is suppressed in wake, and vice versa in sleep. The MA group projects to the cortex and thalamus to determine the overall arousal state of the brain [1,2].

Here each population's activity is summarized in terms of its mean cell body voltage V_j, and mean firing rate Q_j, where $j = m, v$ for MA and VLPO groups, respectively. The firing rate is a sigmoidal function of the voltage, with

$$Q_j(V_j) = \frac{Q_{\max}}{1 + \exp[-(V_j - \theta)/\sigma']}, \tag{1}$$

where $Q_{\max}$ is the maximum possible rate; θ is the mean firing threshold relative to resting and $\sigma'\pi/\sqrt{3}$ is its standard deviation [46]. Dynamics of the mean MA and VLPO neural soma voltages can be represented by

$$\tau_m dV_m/dt = -V_m + \nu_{mv} Q_v + A, \tag{2}$$

$$\tau_v dV_v/dt = -V_v + \nu_{vm} Q_m + D, \tag{3}$$

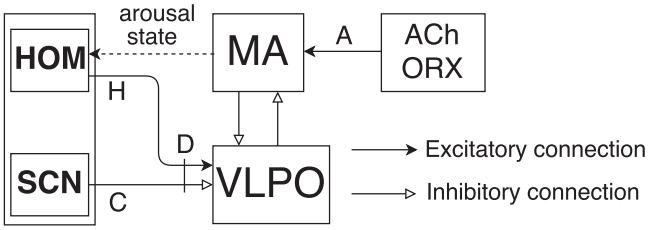

FIG. 1. Components of AAS and their interactions. MA and VLPO populations share a mutually inhibitory connection, with MA active in wake, VLPO active in sleep. The activities of MA and VLPO are respectively enhanced by the drive A from ACh/Orx and the total sleep drive D, which comprises the approximately 24 h periodic circadian drive C from the suprachiasmatic nucleus (SCN) and the homeostatic drive H due to sleep homeostat (HOM). The arousal state also feeds back into homeostatic drive H, eventually triggering sleep [1].

TABLE I. Nominal parameter values for the Phillips-Robinson model. Constraints on these parameters are discussed in Refs. [5,28].

Parameter	Value	Unit	Parameter	Value	Unit
$Q_{\max}$	100	s^{-1}	ν_{vm}	−2.1	mV s
θ	10	mV	ν_{mv}	−1.8	mV s
σ'	3	mV	τ_m	10	s
A	1.3	mV	τ_v	10	s

where τ_j is the characteristic neuromodulatory decay time, ν_{ab} represents the input strength to population a from population b (mutually inhibitory, with $\nu_{mv}, \nu_{vm} < 0$), D is the total sleep drive to the VLPO, and A is a net drive to the MA from cholinergic and orexinergic neurons, which is held constant in the present work. The parameter values used in this paper are listed in Table I and are those obtained in Refs [5,28].

In this model mutual inhibition between wake-promoting (MA) and sleep-promoting (VLPO) nuclei gives rise to a "flip-flop" switch, with each population indirectly reinforcing its own firing by tending to suppress the other population (hence reducing that population's inhibitory effects). Hence, for physiologically reasonable values of the couplings ν_{mv} and ν_{vm} only one population can be active at a time, and the brain is either asleep or awake, with rapid transitions between these states. Thus the steady states of Eqs. (2) and (3) display a saddle-node or fold bifurcation when the MA activity V_m is plotted against the sleep drive D, as shown in Fig. 2. Here V_m is a measure of wakefulness, and its sharp decrease evidences the switch from wake to sleep.

This transition is caused by gradual increase of the sleep drive D, which comprises the approximately 24-h periodic circadian drive C from the suprachiasmatic nucleus (SCN) and the homeostatic drive H due to sleep homeostat (HOM), both afferent to the VLPO as in Fig. 1 [47]). The sleep drive D increases during wake and decreases during sleep [16,48]. The circadian drive C is normally entrained by light, while the homeostatic drive H increases during wake due to the accumulation of somnogens (sleep-promoting chemicals),

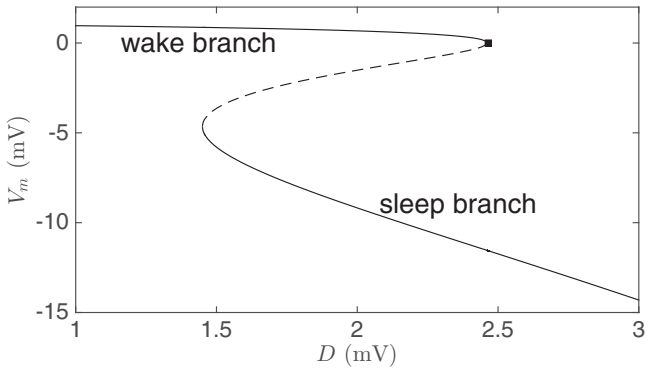

FIG. 2. Steady state value of V_m against the control parameter D shows the saddle-node bifurcation. Stable wake and sleep branches are linked by an unstable branch (dashed line). The square represents the critical transition point of saddle-node bifurcation from wake to sleep. The value of the critical sleep drive is $D_c = 2.463465$ mV, as derived in Sec. III A.

which excite the VLPO. Eventually this stimulus to the VLPO overcomes inhibition by the MA, and the transition to sleep occurs at this critical point, with VLPO activity rising steeply and suppressing the MA. During sleep, somnogens are cleared and H decreases, but the circadian drive C increases during this period. This leads to a flip back to wake once other drives to the MA are sufficient to overcome inhibition by the VLPO.

III. THEORETICAL ANALYSIS

In this section we first simplify the model to a dimensionless form in Sec. III A, then deduce the normal form of dynamics at this critical point in Sec. III B. After that, the power spectrum of fluctuations is calculated in Sec. III C. The scalings of the fluctuation variance and spectral width are quantitively predicted in Sec. III D.

A. Dimensionless form and the critical point

To simplify the dynamics of the Phillips-Robinson model [5], it is convenient to rescale the variables V_m and V_v, and the model parameters, to be dimensionless by introducing new variables defined by

$$u_1 = \frac{V_m - A}{\sigma'}, \tag{4}$$

$$\theta_1 = \frac{\theta - A}{\sigma'}, \tag{5}$$

$$Q_1 = \frac{\nu_{vm} Q_{\max}}{\sigma'}, \tag{6}$$

$$u_2 = \frac{V_v - D}{\sigma'}, \tag{7}$$

$$\theta_2 = \frac{\theta - D}{\sigma'}, \tag{8}$$

$$Q_2 = \frac{\nu_{mv} Q_{\max}}{\sigma'}. \tag{9}$$

After these rescalings, Eqs (2) and (3) become

$$\tau_m \dot{u}_1 + u_1 = S_2(u_2), \tag{10}$$

$$\tau_v \dot{u}_2 + u_2 = S_1(u_1), \tag{11}$$

where S_j is a sigmoid function

$$S_j(u_j) = \frac{Q_j}{1 + \exp(\theta_j - u_j)}, \tag{12}$$

with $j = 1,2$.

For all steady states, $\dot{u}_2 = 0$, whence $u_2 = S_1(u_1)$, which can be inserted into Eq. (10). Then we get

$$\tau_m \dot{u}_1 + u_1 = S_2[S_1(u_1)]. \tag{13}$$

Likewise we have $\dot{u}_1 = 0$ and $u_1 = S_2[S_1(u_1)]$. At the critical states, $\partial \dot{u}_1 / \partial u_1 = 0$, which combined with $\dot{u}_1 = 0$ can give us the critical sleep drive $D_c = 2.463465$ mV for the transition from wake to sleep. We retain a large number of significant figures in our estimate of D_c because we need to compute scalings versus very small departures from this point.

B. Normal form near the critical point of saddle-node bifurcation

In the approach to a critical transition, the dynamical system moves toward a bifurcation at which the dominant real eigenvalue approaches zero. For small deviations from the critical point, a normal form suffices to describe the dynamics around the critical point, with our system being approximated by a mechanical model following Ref. [44].

Around the critical point, the normal form of dynamics is deduced by separating dissipative forces from conservative forces. In this way, Eqs (10) and (11) are reduced to the equation of motion of a particle in a potential well with dissipation, with

$$\tau_m \tau_v \ddot{u}_1 = -\tau_v \dot{u}_1 + \frac{dS_2(u_2)}{du_2} \tau_v \dot{u}_2, \tag{14}$$

$$= -\tau_v \dot{u}_1 + (\tau_m \dot{u}_1 + u_1)\left(1 - \frac{\tau_m \dot{u}_1 + u_1}{Q_2}\right) \times \left[S_1(u_1) + \log\left(\frac{Q_2}{\tau_m \dot{u}_1 + u_1} - 1\right) - \theta_2\right] \tag{15}$$

$$= F_d(\dot{u}_1) + F_c(u_1), \tag{16}$$

where $F_d(\dot{u}_1)$ and $F_c(u_1)$ are the dissipative and conservative forces, respectively.

The form of (15) and its decomposition in (16) can be simplified by making some approximations, as follows: (1) The dissipative force in this system can be shown to be approximately frictional. Taking the partial derivative of Eq. (16) with respect to $\dot{u}_1$ yields [44]

$$\tau_m \tau_v \frac{\partial \ddot{u}_1}{\partial \dot{u}_1} = -(\tau_m + \tau_v) + \tau_m \tau_v \dot{u}_2 \left[1 - \frac{2S_2(u_2)}{Q_2}\right] \tag{17}$$

$$\approx -(\tau_m + \tau_v), \tag{18}$$

with $0 < S_2(u_2)/Q_2 \ll 1$. Figure 3 shows one instance before the wake-sleep transition [49], where we find

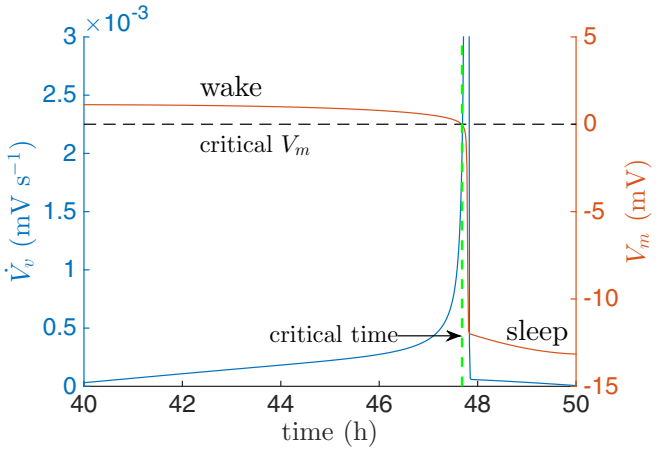

FIG. 3. Time series of the rate $\dot{V}_v$ (blue) and V_m (red) in the wake-sleep transition. The critical value of V_m (dashed black line) can be derived in Sec. III A and indicated by the square point shown in Fig. 2. The critical time for transition from wake to sleep is indicated by the dashed green line. The dynamics of sleep drive D is given in Ref. [49].

$\dot{V}_v < 3 \times 10^{-3}$ mV s^{-1} and then $|\dot{u}_2| = |\dot{V}_v/\sigma'| < 10^{-3}$ s^{-1}. Thus

$$\tau_m \tau_v \dot{u}_2 < 0.1 \text{ s} \ll 20 \text{ s} = \tau_m + \tau_v \tag{19}$$

yields the approximation in Eq. (18). This implies that the dissipative force can be approximated as

$$F_d(\dot{u}_1) \approx -(\tau_m + \tau_v)\dot{u}_1. \tag{20}$$

(2) By setting $\dot{u}_1 = 0$ in Eq. (16), the conservative force can be written as

$$F_c(u_1) = u_1\left(1 - \frac{u_1}{Q_2}\right)\left[S_1(u_1) + \log\left(\frac{Q_2}{u_1} - 1\right) - \theta_2\right] \tag{21}$$

$$\approx u_1\left[S_1(u_1) - \log\left(\frac{u_1}{Q_2}\right) - \theta_2\right], \tag{22}$$

where the approximation is valid for $0 < u_1/Q_2 \ll 1$, because $-1 < u_1 < 0$ and $Q_2 \approx -60$. With this approximation, the critical point for the transition from wake to sleep occurs at $u_1^c = -0.4270$, which is the common solution of $F_c(u_1^c) = 0$ and $F_c'(u_1^c) = 0$ at the critical sleep drive. The corresponding potential of this conservative force can be written as

$$U(u_1) = -\int_{u_1^c}^{u_1} u\left[S_1(u) - \log\left(\frac{u}{Q_2}\right) - \theta_2\right]du. \tag{23}$$

Similarly, by setting $x = u_1 - u_1^c$, Taylor expansion to second order yields

$$F_c(u_1) \approx -a_2(u_1^c)x^2 + a_1(u_1^c)x + a_0(u_1^c), \tag{24}$$

where the values of these coefficients evaluated at u_1^c are given as follows:

$$a_0(u_1^c) = u_1^c(D - D_c)/\sigma', \tag{25}$$

$$a_1(u_1^c) = (D - D_c)/\sigma', \tag{26}$$

$$a_2(u_1^c) = 1/(2u_1^c) - u_1^c S_1''(u_1^c)/2 - S_1'(u_1^c), \tag{27}$$

$$S_1'(u_1^c) = \left.\frac{dS_1}{du_1}\right|_{u_1=u_1^c}, \tag{28}$$

$$S_1''(u_1^c) = \left.\frac{d^2S_1}{du_1^2}\right|_{u_1=u_1^c}. \tag{29}$$

We see that $a_0(u_1^c)$ and $a_1(u_1^c)$ depend linearly on the drive D, whereas $a_2(u_1^c)$ is independent of D.

Actually, when D is near D_c, x is also close to 0. Hence, the drive-dependent linear term $a_1(u_1^c)x$ in Eq. (24) does not significantly change the dynamics, because of its higher-order infinitesimal dependence on $D - D_c$ relative to the term $a_0(u_1^c)$. Thus, around this critical point, it can be omitted and the normal form can be further approximated as

$$m\ddot{x} = -a_2(u_1^c)x^2 + a_0(u_1^c) - \kappa\dot{x}, \tag{30}$$

where $m = \tau_m\tau_v$ is the effective mass of the particle and $\kappa = \tau_m + \tau_v$ is the effective coefficient of friction. Therefore, the wake-sleep system is now converted to a mechanical system of a particle subject to a conservative force and a frictional force $-\kappa\dot{x}$. The potential function for this conservative force can be written as

$$U(x) = ax^3 - bx, \tag{31}$$

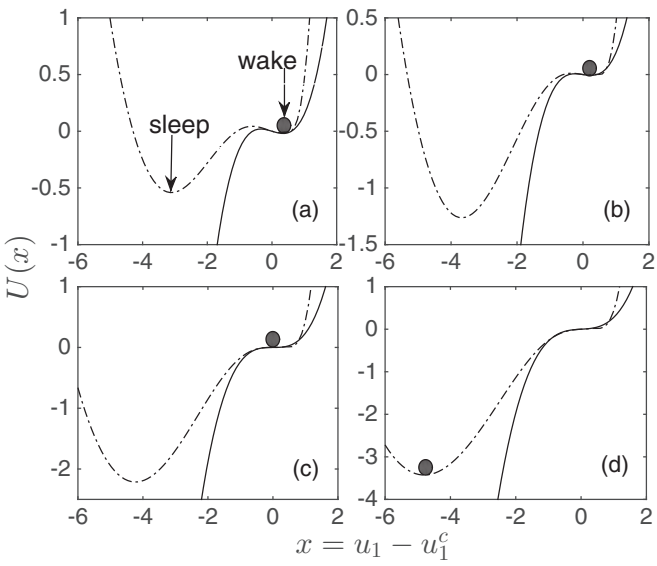

FIG. 4. Variation of the approximate cubic potential $U(x)$ (solid curves) with control parameter b, with the circle in each frame representing the system state. The full potential function of the conservative force $F_c(u_1)$ from Eq. (23) is shown with broken curves. (a) $b > 0$, $D < D_c$: the system is in stable equilibrium corresponding to the wake state ($x > 0$). (b) Same as (a), but D closer to D_c: the potential well is shallow, but the wake state is still stable. (c) $b = 0$, $D = D_c$, the critical transition accompanies loss of stability. (d) $b < 0$, $D > D_c$: the system is in a stable sleep state ($x < 0$).

where $a = a_2(u_1^c)/3 > 0$ and $b = a_0(u_1^c)$ are the parameters that determine the shape of the potential function. Hence,

$$m\ddot{x} = -\frac{\partial U}{\partial x} - \kappa\dot{x} \tag{32}$$

$$= -3ax^2 + b - \kappa\dot{x}, \tag{33}$$

where b acts as a control parameter, linearly related to the sleep drive D, with

$$b = b_0(D_c - D), \tag{34}$$

and $b_0 = -u_1^c/\sigma'$.

If $b > 0$, Fig. 4 shows that the system lies at the stable wake equilibrium at $x > 0$. When it reaches the critical point $b = 0$ (i.e., $D = D_c$), the stable and unstable equilibriums coincide and the system is able to pass through $x = 0$, marking the onset of the critical transition. After that, if b becomes negative, the system moves to a stable sleep state at $x < 0$. A full description of the stable sleep state requires use of the full potential function of the conservative force $F_c(u_1)$ in Eq. (23), which is also shown in Fig. 4. The cubic potential in the above normal form suffices to describe the fluctuating responses, as $b \to 0$, where the steady state is well separated from the sleep state. As b decreases towards 0, the stable potential well flattens, as shown in Fig. 4(c). This implies that, analogous to the simple harmonic oscillator, the restoring force weakens, thereby resulting in higher fluctuation amplitudes and lower characteristic frequencies.

C. Power spectrum

If the particle is driven by a normalized random force, the response of Eq. (33) can be Fourier transformed to obtain the power spectrum of the response fluctuations, as detailed in the Appendix. The result is

$$P(\omega) = \frac{1}{m^2\left({\omega_1}^2 - \omega^2\right)^2 + \omega^2\kappa^2}, \tag{35}$$

where

$$\omega_1 = \alpha(D_c - D)^{1/4} \tag{36}$$

is the characteristic frequency of harmonic motion in the potential well with $\alpha = (12ab_0)^{1/4}/\sqrt{m}$, dependent only on the parameters of the potential and the effective mass of the dynamical system.

The denominator of power spectrum in Eq. (35) can be expressed as

$$f(\omega) = m^2\left({\omega_1}^2 - \omega^2\right)^2 + \omega^2\kappa^2 \tag{37}$$

$$= m^2\left[\omega^2 - \left({\omega_1}^2 - \frac{\kappa^2}{2m^2}\right)\right]^2 + {\omega_1}^2\kappa^2 - \frac{\kappa^4}{4m^2}, \tag{38}$$

which indicates that if ${\omega_1}^2 - \kappa^2/(2m^2) > 0$, there is a minimal value of $f(\omega)$ and hence a resonance at the frequency

$$\omega_r = \sqrt{{\omega_1}^2 - \kappa^2/(2m^2)}. \tag{39}$$

However, from Eq. (36), ω_1 can be arbitrarily small if D is close enough to D_c, so no resonance appears when the system is sufficiently close to the critical point. Actually, in our simulation in Sec. IV A, we choose $\log_{10}(D_c - D) \leqslant -2$ and $\kappa/m = 0.2\ \mathrm{s}^{-1}$, so

$$\omega_1 \leqslant (10^{-2})^{1/4}\alpha = 0.0252\ \mathrm{s}^{-1} \ll \kappa/m, \tag{40}$$

which implies that the dissipation is large enough to prevent any resonance when the steady state is close enough to the critical one, as in the cases we consider.

Therefore, as shown in Fig. 5(a), we can divide the spectrum into the following three regimes:

(1) A plateau for $\omega \ll \omega_1$. In this regime, the theoretical power spectrum in Eq. (35) can be simplified to

$$P(\omega) \approx \frac{1}{m^2{\omega_1}^4} \sim (D_c - D)^{-1}, \tag{41}$$

which is independent of ω. Equation (41) also indicates that the power at low frequency increases as the sleep drive D approaches the critical point D_c.

(2) If $\omega \ll \omega_1$ is not satisfied, but ω is close to ω_1, that is $|\omega - \omega_1| \ll \kappa/m$, then we get a shallow power-law regime. In this regime, the first term in the denominator of Eq. (35) can be neglected, yielding

$$P(\omega) \approx \frac{1}{\kappa^2\omega^2} \sim \omega^{-2}, \tag{42}$$

which is shown as the black dashed line in Fig. 5. Notice that such scaling behavior can also be indicated by the asymptotic trend of points $(\omega_1/2\pi,\ P(\omega_1))$ for various values of $\log_{10}(D_c - D)$, marked by $\times$ symbols in Fig. 5(a). This is because, from Eq. (35), the power at $\omega = \omega_1$ can be calculated to be $P(\omega_1) = 1/(\kappa^2{\omega_1}^2)$.

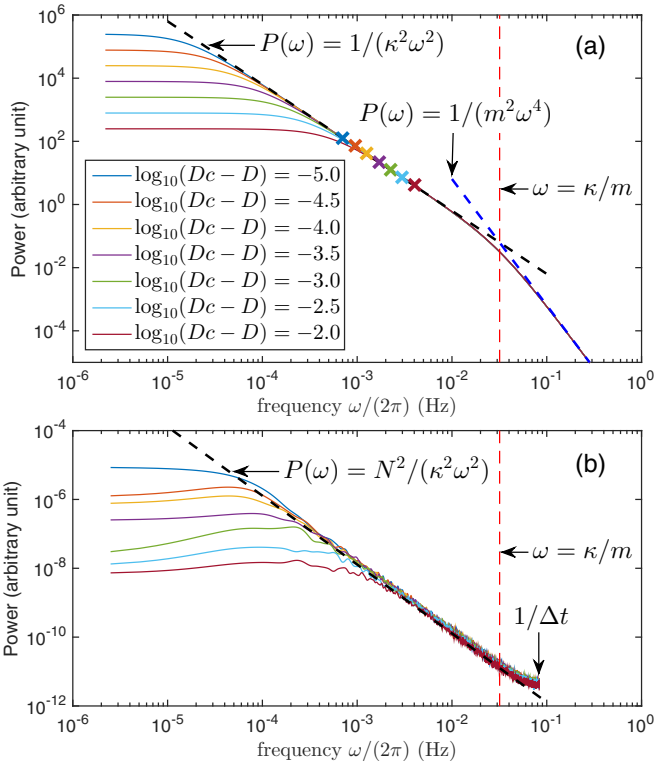

FIG. 5. Log-log plots of power spectrum for various values of $\log_{10}(D_c - D)$. (a) Theoretical power spectra from Eq. (35). For each curve, the point $[\omega_1/2\pi,\ P(\omega_1)]$ is marked by a $\times$ symbol in the same color as the corresponding curve. The red vertical line represents $\omega = \kappa/m$. The black and blue dashed lines are power-law scalings of the form ω^{-2} and ω^{-4}, respectively. Parameters are $m = 100\ \mathrm{s}^2$, $\kappa = 20\ \mathrm{s}$, and $\alpha = 0.0796\ \mathrm{mV}^{-1/4}\ \mathrm{s}^{-1}$. (b) Power spectra from numerical simulations, driven by external white noise with small amplitude $c = 10^{-4}$ mV, which is input to the VLPO voltage V_v. They are smoothed by local averaging over frequency for clarity. The particle is driven by a random force with amplitude $N = -u_1^c c/\sigma' \approx 1.42 \times 10^{-5}$. The maximal frequency included in the simulations is given by $1/\Delta t$ with the simulation time step $\Delta t = 12\ \mathrm{s}$.

(3) A steep power-law regime for $\omega \gg \kappa/m \gg \omega_1$. In this regime, $P(\omega) \approx 1/(m^2\omega^4)$, and thus the rapid drop of the power at high frequency ultimately steepens to a scaling of ω^{-4}. Such asymptotic behavior is also shown as the blue dashed line in Fig. 5(a).

D. Theoretical scalings

We now calculate the scalings of the fluctuation variance and spectral width versus $D_c - D$.

The variance can be calculated by integrating the power spectrum over all frequencies:

$$\sigma^2 = \int_0^\infty P(\omega)\,d\omega = \frac{\pi}{2m\kappa{\omega_1}^2}. \tag{43}$$

This integral is evaluated in the Appendix, giving

$$\sigma^2 \sim (D_c - D)^\beta, \tag{44}$$

with $\beta = -1/2$. Alternatively, this scaling behavior can be understood by a heuristic derivation without friction ($\kappa = 0$), which is also given in the Appendix.

Following Ref. [40], the spectral width w can be defined to be the angular frequency below which a given fraction of the total fluctuation power resides. Here we choose this fraction to be 0.75, as in Ref. [40], so w is the solution of

$$0.75\sigma^2 = \int_0^w P(\omega)\, d\omega. \tag{45}$$

The scaling of w versus $D_c - D$ can be estimated based on the shape of power spectrum. Since the power is dominated by the low frequency, such as $\omega \ll \omega_1$, the integral in Eq. (45) can be approximated by

$$0.75\sigma^2 \approx w P(0), \tag{46}$$

which from Eq. (41) leads to the scaling

$$w \sim {\omega_1}^4 \sigma^2 \sim (D_c - D)^\gamma, \tag{47}$$

with $\gamma = 1/2$.

IV. COMPARISON OF SIMULATION RESULTS WITH THEORETICAL PREDICTIONS

In this section we use numerical methods to simulate Eqs. (1)–(3) to compare with the theoretical results. The comparison of theoretical power spectrum with the simulated one is presented in Sec. IV A, and the scalings are discussed in Sec. IV B.

A. Simulated power spectrum

In this work, the combined cholinergic and orexinergic drive A (see Fig. 1) is held constant. The transition from wake to sleep is then approached by increasing the sleep drive D toward its critical level D_c in small steps. At each step the system has a particular fixed sleep drive value D, which produces a statistically stable MA voltage signal. To restrict the system around the wake state, each initial value is set as the previous final one. Any residual transient effects are then removed by disregarding the first part of each time series. Here each run has 12-s time steps and continues for more than 1000 h with the first 500 h removed, and we do two runs for each D. The data from these two runs are uniformly split into a total 50 time series, each of which is Fourier transformed to obtain the power spectrum, and then averaged to give the mean power spectrum plotted in Fig. 5(b). In our simulations, $\log_{10}(D_c - D)$ varies between -2 and -5 in steps of 0.1.

In each run, an independent white noise signal is added to the VLPO voltage V_v, with the noise amplitude kept small enough that it comes nowhere near inducing a state transition. Specifically, the noise amplitude is set as $c = 10^{-4}$ mV, in contrast with the minimal distance from the transition

$$\Delta V_v \approx \sigma' S_1'\left(u_1^c\right)\Delta u_1 \approx 1.97 \times 10^{-2}\ \text{mV}, \tag{48}$$

which corresponds to the minimal width of the potential well

$$\Delta u_1 = 2\sqrt{b/(3a)} \approx 2.8 \times 10^{-3}, \tag{49}$$

at $D_c - D = 10^{-5}$. Therefore, the system driven by this small noise will stay at the wake state.

With the noise input to V_v, $u_2(t)$ is replaced by $u_2(t) + c/\sigma'\xi(t)$ in Eqs. (2) and (3), where $\xi(t)$ is the normalized white noise. In the low-frequency regime, this is equivalent to the particle being perturbed by a random force $N\xi(t)$ with its amplitude

$$N = -u_1^c c/\sigma' \approx 1.42 \times 10^{-5}, \tag{50}$$

and the dynamics of the particle can be given as

$$m\ddot{x}(t) + \kappa\dot{x}(t) + \frac{\partial U}{\partial x} = N\xi(t). \tag{51}$$

From Fig. 5(b), we can find that for each value of $\log_{10}(D_c - D)$, the simulated power spectrum consists of a plateau at low frequency and the regime of power-law scaling

$$P(\omega) = \frac{N^2}{\kappa^2\omega^2}. \tag{52}$$

Therefore, in the low-frequency regime, our simulated power spectrum agree well with the theoretical prediction as shown in Fig. 5(a).

However, as shown in Fig. 5(b), the simulated power shows a slight turnup in the high-frequency regime $\omega > \kappa/m$, instead of the rapid drop in the predicted power spectrum in Fig. 5(a). This difference may be due to the large simulation time step $\Delta t = 12$ s, which limits the simulated frequency to be less than $1/\Delta t \approx 0.08$ Hz and is also the coherent time scale of the input noise. The increased coherence may enhance the power of this frequency regime close to $1/\Delta t$.

Nonetheless, their difference has little effect on the scalings of variance and spectral width as the sleep drive D approaches the critical point D_c, as presented below. The reason is that both of them are dominated by low-frequency components with high power.

B. Scalings

Similarly to Ref. [40], our scaling analyses of variance and critical slowing down are based on the power spectrum, where the height of plateau increases but its width decreases as the sleep drive $D \to D_c$, as shown in Fig. 5. This indicates that the noise-induced fluctuations grow in amplitude and decay in frequency.

The numerical variance and spectral width are plotted against $D_c - D$ in Fig. 6. Both show the following power-law scalings

$$\sigma^2 \sim (D_c - D)^\beta, \tag{53}$$

$$w \sim (D_c - D)^\gamma. \tag{54}$$

We estimate the scaling exponents by weighted linear least-squares fitting on a log-log scale. Because the theoretical exponents only apply rigorously in the limit $D \to D_c$, we examine fits using a sliding window that includes half the total 32 points investigated, which were equally spaced logarithmically between $D_c - D = 10^{-5}$ and 10^{-2}. The fit is done first over the points nearest to 10^{-2}, and then the window is moved toward smaller $D_c - D$, progressively discarding the points further from D_c and including the ones closer. Weighted linear fitting is performed with a weight $W = W_e W_k$, where W_e is an error-based weight, inversely proportional to the square

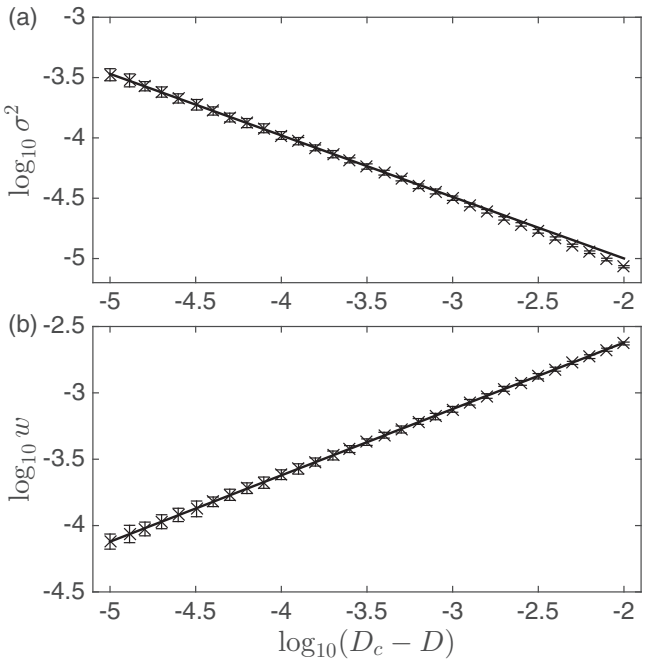

FIG. 6. Log-log plots of variance and spectral width against the distance $D_c - D$, with error bars calculated as the standard deviation of the measurements over 50 runs. The line is the best weighted linear fitting on the log-log scale. (a) Variance vs $D_c - D$. (b) Spectral width vs $D_c - D$.

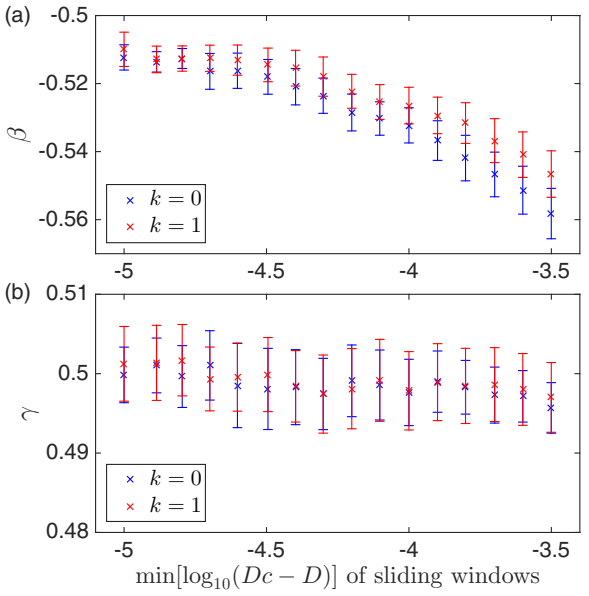

FIG. 7. Scaling exponents fitted on data points of moving windows against their minimal values of $\log_{10}(D_c - D)$. Error bars are given by bounds of 95% confidence interval in the weighted linear fitting in Fig. 6. (a) variance; (b) spectral width.

of the error ϵ as $W_e = 1/\epsilon^2$, while W_k is a linearly skewed weight function with a relative slope of k within the sliding window to enable points nearer D_c to be further emphasized by choosing larger k. Specifically, for each point (X,Y), the skewed weight W_k assigned to Y is expressed as

$$W_k = 1 - k\frac{X - X_{\text{mid}}}{X_{\text{max}} - X_{\text{mid}}}, \tag{55}$$

where X_{min}, X_{max}, and X_{mid} are the smallest, largest, and middle values of $\log_{10}(D_c - D)$ in the sliding window. Additionally, k is restricted to the range from 0 to 1, to ensure no negative weights, thereby yielding a uniform weight function at $k = 0$ and a triangular profile at $k = 1$.

As shown in Fig. 7, both exponents are close to their theoretical predictions of $\beta = -1/2$ and $\gamma = 1/2$ in Sec. III D, especially when the sliding window is close to D_c and the weights are skewed toward D_c. Our best numerical estimates are $\beta = 0.510 \pm 0.006$ and $\gamma = 0.501 \pm 0.005$, and their agreement with theory is likely to improve further at lower $D_c - D$.

V. SUMMARY AND DISCUSSION

We have derived nondimensional and normal forms of the dynamics of the ascending arousal system that governs the sleep-wake cycle in a way that retains the explicit links between the coefficients of the normal form and the underlying physiology. This has been used to explore the dynamics and scaling properties of the system in the presence of noise near the saddle-node bifurcation that marks the transition from wake to sleep, using both theoretical and numerical approaches. The main results are the following:

(1) A dimensionless normal form was derived that expresses the dynamics in terms of motion of a particle in a frictional quadratic potential, thereby placing earlier results in a tractable form for further analysis.

(2) The power spectrum for the noise-driven system was derived, showing a low-frequency plateau that narrows toward zero width as the system approaches the critical point D_c of the sleep drive D for the wake-sleep transition. This is followed by an ω^{-2} regime that steepens to ω^{-4} when friction dominates at high frequencies.

(3) Scalings of the variance and spectral width of the noise-driven fluctuations were derived. The variance was predicted to scale as $(D_c - D)^{-1/2}$, consistent with large critical-point fluctuations. The spectral width was predicted to scale as $(D_c - D)^{1/2}$, due to critical slowing down. Numerical simulations yielded best-estimate exponents very close to the theoretical predictions, especially when based on simulations nearest to D_c.

We have focused on the analysis near the critical point to investigate the potential precursors. The present work is thus not concern with other multiscale phenomena, such as transient oscillations and waves, which are sometimes detected by fitting nonphysiological linear autoregressive (AR) statistical models with time-dependent parameters [50], or by analyzing cross-modulation of amplitudes and frequencies in ranges relevant to electroencephalography, for example [51]. The two key phenomena associated with critical transitions, increased variability and critical slowing down, can also be detected by a variety of statistical and data analysis methods [41], but we stress that our approach is founded firmly in the underlying physiology in the present case. In other works

the autocorrelation (AC) function and detrended fluctuation analysis (DFA) have also been applied to critical points in climate tipping with some success [35,39]. Interestingly, the scaling properties using AC function and DFA can actually be interpreted via spectral analysis, using a weighted integral over the power spectrum [52], so they are not independent measures.

Overall, it is expected that critical fluctuations and their slowing will provide useful precursors to the wake-sleep transition for use in practical situations such as transport and safety-related occupations where warning of imminent loss of alertness is of great importance. Here and more generally, it will be necessary to extend our analysis and simulations to incorporate the effects of variation of D over time, and of non-negligible variance of input noise. The former effect requires us to relax the quasisteady assumption, which will limit how clearly different time scales can be separated. The latter effect may lead to phenomena such as flickering between bistable states and early or delayed onset of critical transitions [41,53,54] and may play a role in narcolepsy and microsleeps [47]. Future work will thus involve incorporating rates of change and noise parameters from experiment.

This novel application of bifurcation theory to the field of neuroscience provides insight into the underlying mechanism of wake-sleep transition and validates the use of similar methods to investigate potential precursors to other catastrophic bifurcations, e.g., sleep-wake transition, with the hope of predicting the transition itself, as well as gaining an understanding of pretransition phenomena. More generally, such a switch with all-or-none bistability is prevalent in a host of systems; some biological ones include cell cycle progression [55], cellular differentiation [56], apoptosis [57], *Xenopus* oocyte maturation [58], mammalian calcium signal transduction [59], and polarity in budding yeast [60].

ACKNOWLEDGMENTS

This work was supported by the Australian Research Council Center of Excellence for Integrative Brain Function (ARC Grant CE140100007) and the Australian Research Council Laureate Fellowship Grant (ARC Grant FL140100025).

APPENDIX: VARIANCE SCALING

In this appendix, the variance scaling is derived in two ways: a heuristic derivation with no friction and a detailed derivation based on the power spectrum.

1. Variance scaling with no friction

For a heuristic derivation of variance scaling, set $\kappa = 0$ in Eq. (33). By linearizing around the potential minimum at $x_0 = \sqrt{b/3a}$ and setting $y = x - x_0$, Eq. (33) becomes

$$\frac{d^2y}{dt^2} = -{\omega_1}^2 y, \tag{A1}$$

with $\omega_1 = \sqrt{(12ab)^{1/2}/m}$, representing simple harmonic motion at an angular frequency ω_1, when $b > 0$. Thus we obtain

$$\omega_1 = \alpha(D_c - D)^{1/4}, \tag{A2}$$

with $\alpha = \sqrt{(12ab_0)^{1/2}/m}$ dependent only on constants that define the underlying potential and the effective mass of the dynamical system. Thus $\omega_1 \sim (D_c - D)^{1/4}$ indicates critical slowing down as $D \to D_c$.

Now, if the energy of the particle is an amount ΔU above the bottom of the well, we note that

$$\Delta U \approx \frac{d^2U(x)}{dx^2}M^2 = -(12ab)^{1/2}M^2, \tag{A3}$$

where M is the amplitude of oscillation and the derivative is evaluated at x_0. Hence, if the energy is constant, we find

$$M^2 \sim (D_c - D)^{-1/2}, \tag{A4}$$

and this is the scaling of any quantity that has the dimension of a positional variance.

2. Theoretical spectrum and scaling

Taking $\kappa \neq 0$ in Eq. (33), in a similar way to the last section, we find

$$m\frac{d^2y}{dt^2} + \kappa\frac{dy}{dt} + m{\omega_1}^2 y = \xi(t), \tag{A5}$$

where we have added white noise $\xi(t)$ on the right side.

By Fourier transforming Eq. (A5), we obtain

$$\left(-m\omega^2 - i\omega\kappa + m{\omega_1}^2\right)y(\omega) = 1. \tag{A6}$$

Rearranging Eq. (A6) and squaring its modulus yields the total

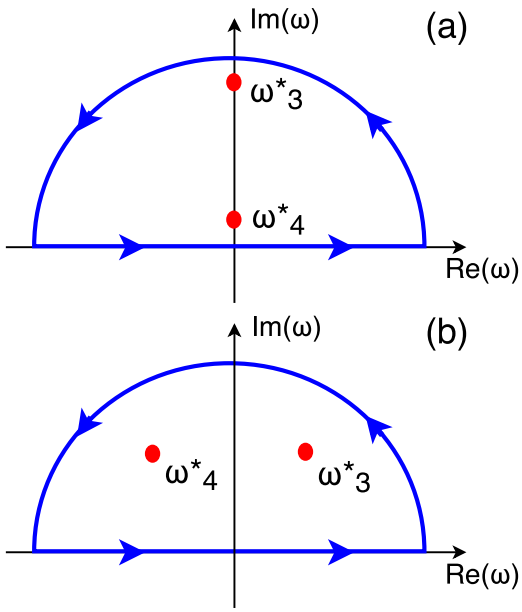

FIG. 8. Sketch of contour integrations used to evaluate (A9). The integration extends around the blue contour in the direction indicated and is evaluated via the residues at poles of $P(\omega)$ that it encircles (red circles). When evaluating the integral, the limit is taken in which the semicircular part of the contour becomes infinite in radius. (a) Case with two poles on the imaginary axis. (b) Case with two poles with equal and opposite nonzero real parts.

power in system fluctuations in response to white noise drive with unit amplitude:

$$P(\omega) = |y(\omega)|^2 = \frac{1}{m^2\left(\omega_1{}^2 - \omega^2\right)^2 + \omega^2\kappa^2}, \tag{A7}$$

where the normalized noise was used. Parseval's theorem implies that the fluctuation variance is proportional to P.

The total power in system fluctuations is obtained by integrating Eq. (A7) over ω as follows:

$$P = \int_0^\infty P(\omega)\, d\omega, \tag{A8}$$

$$= \frac{1}{2}\int_{-\infty}^{\infty} \frac{d\omega}{m^2\left(\omega_1{}^2 - \omega^2\right)^2 + \omega^2\kappa^2}, \tag{A9}$$

which can be easily evaluated by contour integration. The poles of the integrand lie at

$$\omega^*_{1,2} = \left(-i\kappa \pm \sqrt{-\kappa^2 + 4m^2\omega_1{}^2}\right)/2m, \tag{A10}$$

$$\omega^*_{3,4} = \left(i\kappa \pm \sqrt{-\kappa^2 + 4m^2\omega_1{}^2}\right)/2m. \tag{A11}$$

We perform the contour integration along the upper half of the circle centered at the origin, with the semicircular segment taken to infinity, as shown in Fig. 8. Hence we are interested in the poles $\omega^*_{3,4}$ in the upper half plane. For $\kappa^2 > 4m^2\omega_1{}^2$, these two poles occur on the imaginary axis as shown in Fig. 8(a); in the opposite case, as shown in Fig. 8(b), $\omega^*_{3,4} = -i\kappa/2m \pm r$ where r is real.

The contour integral is calculated by evaluating the residues at the poles. This yields

$$P = \frac{\pi}{2\kappa m\omega_1{}^2} \tag{A12}$$

for all values of κ^2. This result has the same scaling as heuristic one in Eq. (A4).

[1] C. B. Saper, T. C. Chou, and T. E. Scammell, The sleep switch: Hypothalamic control of sleep and wakefulness, Trends Neurosci. **24**, 726 (2001).

[2] R. E. Brown, R. Basheer, J. T. McKenna, R. E. Strecker, and R. W. McCarley, Control of sleep and wakefulness, Physiol. Rev. **92**, 1087 (2012).

[3] C. B. Saper, G. Cano, and T. E. Scammell, Homeostatic, circadian, and emotional regulation of sleep, J. Comp. Neurol. **493**, 92 (2005).

[4] P. A. Robinson, A. J. K. Phillips, B. D. Fulcher, M. Puckeridge, and J. A. Roberts, Quantitative modeling of sleep dynamics, Phil. Trans. R. Soc. A **369**, 3840 (2011).

[5] A. J. K. Phillips and P. A. Robinson, A quantitative model of sleep-wake dynamics based on the physiology of the brainstem ascending arousal system, J. Biol. Rhythms **22**, 167 (2007).

[6] P. A. Robinson, S. Postnova, R. G. Abeysuriya, J. W. Kim, J. A. Roberts, L. McKenzie-Sell, A. Karanjai, C. C. Kerr, F. Fung, R. Anderson, M. J. Breakspear, P. M. Drysdale, B. D. Fulcher, A. J. K. Phillips, C. J. Rennie, and G. Yin, A multiscale "working brain" model, in *Validating Neuro-Computational Models of Neurological and Psychiatric Disorders*, Springer Series in Computational Neuroscience, Vol. 14, edited by B. S. Bhattacharya and F. N. Chowdhury (Springer International, New York, 2015), pp. 107–140.

[7] J. Virkkala, J. Hasan, A. Värri, S.-L. Himanen, and K. Müller, Automatic sleep stage classification using two-channel electro-oculography, J. Neurosci. Methods **166**, 109 (2007).

[8] T. Åkerstedt and M. Gillberg, Subjective and objective sleepiness in the active individual, Int. J. Neurosci. **52**, 29 (1990).

[9] W. C. Dement and M. M. Mitler, It's time to wake up to the importance of sleep disorders, JAMA **269**, 1548 (1993).

[10] J. A. Horne and L. A. Reyner, Sleep related vehicle accidents, BMJ **310**, 565 (1995).

[11] M. Johns and B. Hocking, Daytime sleepiness and sleep habits of australian workers, SLEEP-NEW YORK **20**, 844 (1997).

[12] J. M. Lyznicki, T. C. Doege, R. M. Davis, and M. A. Williams, Sleepiness, driving, and motor vehicle crashes, JAMA **279**, 1908 (1998).

[13] P. Achermann, D.-J. Dijk, D. P. Brunner, and A. A. Borbély, A model of human sleep homeostasis based on EEG slow-wave activity: Quantitative comparison of data and simulations, Brain Res. Bull **31**, 97 (1993).

[14] A. A. Borbely and P. Achermann, Sleep homeostasis and models of sleep regulation, J. Biol. Rhythms **14**, 559 (1999).

[15] M. E. Jewett and R. E. Kronauer, Interactive mathematical models of subjective alertness and cognitive throughput in humans, J. Biol. Rhythms **14**, 588 (1999).

[16] A. Borbely and P. Achermann, in *Principles and Practice of Sleep Medicine*, 3rd ed., edited by M. Kyger, T. Roth, and W. Dement (Saunders, Philadelphia, 2000), pp. 377–390.

[17] P. Achermann and A. A. Borbély, Mathematical models of sleep regulation, Front. Biosci. **8**, s683 (2003).

[18] Y. Tamakawa, A. Karashima, Y. Koyama, N. Katayama, and M. Nakao, A quartet neural system model orchestrating sleep and wakefulness mechanisms, J. Neurophysiol. **95**, 2055 (2006).

[19] S. Postnova, K. Voigt, and H. A. Braun, A mathematical model of homeostatic regulation of sleep-wake cycles by hypocretin/orexin, J. Biol. Rhythms **24**, 523 (2009).

[20] M. J. Rempe, J. Best, and D. Terman, A mathematical model of the sleep/wake cycle, J. Math. Biol. **60**, 615 (2010).

[21] R. Kumar, A. Bose, and B. N. Mallick, A mathematical model towards understanding the mechanism of neuronal regulation of wake-NREMS-REMS states, PLoS One **7**, e42059 (2012).

[22] V. Booth and C. G. D. Behn, Physiologically-based modeling of sleep–wake regulatory networks, Math. Biosci. **250**, 54 (2014).

[23] A. C. Skeldon, D.-J. Dijk, and G. Derks, Mathematical models for sleep-wake dynamics: Comparison of the two-process model and a mutual inhibition neuronal model, PloS One **9**, e103877 (2014).

[24] S. Bañuelos, J. Best, G. Huguet, A. Prieto-Langarica, P. B. Pyzza, M. H. Schmidt, and S. Wilson, Effects of

thermoregulation on human sleep patterns: A mathematical model of sleep–wake cycles with REM–NREM subcircuit, in *Applications of Dynamical Systems in Biology and Medicine* edited by T. Jackson and A. Radunskaya (Springer, New York, 2015), pp. 123–147.

[25] M. Patel, A simplified model of mutually inhibitory sleep-active and wake-active neuronal populations employing a noise-based switching mechanism, J. Theor. Biol. **394**, 127 (2016).

[26] M. S. Costa, J. Born, J. C. Claussen, and T. Martinetz, Modeling the effect of sleep regulation on a neural mass model, J. Comput. Neurosci. **41**, 15 (2016).

[27] B. D. Fulcher, A. Phillips, S. Postnova, and P. A. Robinson, A physiologically based model of orexinergic stabilization of sleep and wake, PloS One **9**, e91982 (2014).

[28] A. J. K. Phillips and P. A. Robinson, Sleep deprivation in a quantitative physiologically based model of the ascending arousal system, J. Theor. Biol. **255**, 413 (2008).

[29] B. D. Fulcher, A. J. K. Phillips, and P. A. Robinson, Quantitative physiologically based modeling of subjective fatigue during sleep deprivation, J. Theor. Biol. **264**, 407 (2010).

[30] M. Puckeridge, B. D. Fulcher, A. J. K. Phillips, and P. A. Robinson, Incorporation of caffeine into a quantitative model of fatigue and sleep, J. Theor. Biol. **273**, 44 (2011).

[31] A. J. K. Phillips, P. A. Robinson, D. J. Kedziora, and R. G. Abeysuriya, Mammalian sleep dynamics: How diverse features arise from a common physiological framework, PLoS Comput. Biol. **6**, e1000826 (2010).

[32] M. Scheffer, J. Bascompte, W. A. Brock, V. Brovkin, S. R. Carpenter, V. Dakos, H. Held, E. H. van Nes, M. Rietkerk, and G. Sugihara, Early-warning signals for critical transitions, Nature (London) **461**, 53 (2009).

[33] V. A. Dubrovskii and V. N. Sergeev, Universal precursor of geomechanical catastrophes, Dokl. Phys. **49**, 231 (2004).

[34] V. A. Dubrovskiy and V. N. Sergeev, Short- and medium-term earthquake precursors as evidence of the sliding instability along faults, Izvestiya-Phys. Solid Earth **42**, 802 (2006).

[35] V. N. Livina and T. M. Lenton, A modified method for detecting incipient bifurcations in a dynamical system, Geophys. Res. Lett. **34** (2007).

[36] V. Dakos, M. Scheffer, E. H. van Nes, V. Brovkin, V. Petoukhov, and H. Held, Slowing down as an early warning signal for abrupt climate change, Proc. Natl. Acad. Sci. U.S.A. **105**, 14308 (2008).

[37] J. M. T. Thompson and J. Sieber, Climate tipping as a noisy bifurcation: A predictive technique, IMA J. Appl. Math. **76**, 27 (2011).

[38] J. Sieber and J. M. T. Thompson, Nonlinear softening as a predictive precursor to climate tipping, Phil. Trans. R. Soc. A **370**, 1205 (2012).

[39] T. M. Lenton, V. N. Livina, V. Dakos, E. H. van Nes, and M. Scheffer, Early warning of climate tipping points from critical slowing down: Comparing methods to improve robustness, Phil. Trans. R. Soc. A **370**, 1185 (2012).

[40] R. D. Peters, M. Le Berre, and Y. Pomeau, Prediction of catastrophes: An experimental model, Phys. Rev. E **86**, 026207 (2012).

[41] M. Scheffer, S. R. Carpenter, T. M. Lenton, J. Bascompte, W. Brock, V. Dakos, J. van de Koppel, I. A. van de Leemput, S. A. Levin, E. H. van Nes, M. Pascual, and J. Vandermeer, Anticipating critical transitions, Science **338**, 344 (2012).

[42] M. A. Kramer, W. Truccolo, U. T. Eden, K. Q. Lepage, L. R. Hochberg, E. N. Eskandar, J. R. Madsen, J. W. Lee, A. Maheshwari, E. Halgren, C. J. Chu, and S. S. Cash, Human seizures self-terminate across spatial scales via a critical transition, Proc. Natl. Acad. Sci. U.S.A. **109**, 21116 (2012).

[43] M. Iwata and S. I. Sasa, Scale-free patterns at a saddle-node bifurcation in a stochastic system, Phys. Rev. E **78**, 055202 (2008).

[44] A. J. K. Phillips and P. A. Robinson, Potential formulation of sleep dynamics, Phys. Rev. E **79**, 021913 (2009).

[45] C. Wissel, A universal law of the characteristic return time near thresholds, Oecologia **65**, 101 (1984).

[46] P. A. Robinson, C. J. Rennie, and J. J. Wright, Propagation and stability of waves of electrical activity in the cerebral cortex, Phys. Rev. E **56**, 826 (1997).

[47] P. A. Robinson, C. J. Rennie, A. J. K. Phillips, J. W. Kim, and J. A. Roberts, Phase transitions in physiologically-based multiscale mean-field brain models, in *Modeling Phase Transitions in the Brain*, Springer Series in Computational Neuroscience, Vol. 4, edited by D. A. Steyn-Ross and M. Steyn-Ross (Springer, New York, 2010), pp. 179–201.

[48] C. Czeisler and S. Khalsa, in *Principles and Practice of Sleep Medicine*, 3rd ed., edited by M. Kyger, T. Roth, and W. Dement (Saunders, Philadelphia, 2000), pp. 353–375.

[49] B. D. Fulcher, A. J. K. Phillips, and P. A. Robinson, Modeling the impact of impulsive stimuli on sleep-wake dynamics, Phys. Rev. E **78**, 051920 (2008).

[50] E. Olbrich and P. Achermann, Analysis of oscillatory patterns in the human sleep EEG using a novel detection algorithm, J. Sleep Res. **14**, 337 (2005).

[51] F. Gans, A. Y. Schumann, J. W. Kantelhardt, T. Penzel, and I. Fietze, Cross-Modulated Amplitudes and Frequencies Characterize Interacting Components in Complex Systems, Phys. Rev. Lett. **102**, 098701 (2009).

[52] P. A. Robinson, Interpretation of scaling properties of electroencephalographic fluctuations via spectral analysis and underlying physiology, Phys. Rev. E **67**, 032902 (2003).

[53] H. B. Chan and C. Stambaugh, Activation barrier scaling for fluctuation induced switching in driven non-linear micromechanical oscillators, J. Stat. Mech. Theor. Exp. (2009) P01028.

[54] J. P. Eckmann, L. Thomas, and P. Wittwer, Intermittency in the presence of noise, J. Phys. A **14**, 3153 (1981).

[55] J. J. Tyson and B. Novak, Temporal organization of the cell cycle, Curr. Biol. **18**, R759 (2008).

[56] A. Ghaffarizadeh, N. S. Flann, and G. J. Podgorski, Multistable switches and their role in cellular differentiation networks, BMC Bioinform. **15**, S7 (2014).

[57] K. L. Ho and H. A. Harrington, Bistability in apoptosis by receptor clustering, PLoS Comput. Biol. **6**, e1000956 (2010).

[58] J. E. Ferrell and E. M. Machleder, The biochemical basis of an all-or-none cell fate switch in xenopus oocytes, Science **280**, 895 (1998).

[59] A. M. Zhabotinsky, Bistability in the Ca^{2+}/calmodulin-dependent protein kinase-phosphatase system, Biophys. J **79**, 2211 (2000).

[60] Y. Mori, A. Jilkine, and L. Edelstein-Keshet, Wave-pinning and cell polarity from a bistable reaction-diffusion system, Biophys. J **94**, 3684 (2008).